Degradation mechanism of tributyl phosphate by UV/H2O2 treatment and parameters optimization towards the design of a pilot reactor

Thibault d'Halluin, Célia Lepeytre, Antoine Leydier, Carine Julcour-Lebigue

https://doi.org/10.1080/09593330.2020.1751731

Degradation mechanism of tributyl phosphate by UV/H_2O_2 treatment and parameters optimization towards the design of a pilot reactor

Thibault D'halluin[a,b], Célia Lepeytre[a], Antoine Leydier[a] and Carine Julcour[b]

[a]Decontamination and Supercritical Processes Laboratory BP17171, CEA, DEN, Univ Montpellier, DE2D, SEAD, Bagnols-sur-Ceze, France; [b]Laboratoire de Génie Chimique, Université de Toulouse, CNRS, INPT, UPS, Toulouse, France

ABSTRACT

While activated sludge treatment is currently the preferred process for the removal of tributyl phosphate (TBP) at the mg.L^{-1} level, it is well known that this recalcitrant molecule is incompletely degraded, stimulating research into alternative approaches, such as advanced oxidation. The aim of this study was to characterize the degradation mechanism of TBP during ultraviolet/H_2O_2 treatment using ^{31}P NMR, ionic chromatography and total organic carbon analysis. The effects of initial pH, amount of oxidant and pollutant concentration were also assessed using an experimental design approach. The results of this parametric study show that ultraviolet/H_2O_2 photo-oxidation efficiently degrades TBP at concentrations up to 600 mg.L^{-1}, with >90% phosphate release and up to 95% removal of total organic carbon within 1 h. The data also show that the main reaction intermediates are short carboxylic acids, resulting from the released alkyl groups, meaning that an interesting application of this process may be to rapidly pre-treat industrial effluent upstream of activated sludge reactors.

KEYWORDS

Water treatment; organophosphates; AOP; photo-oxidation; degradation mechanism

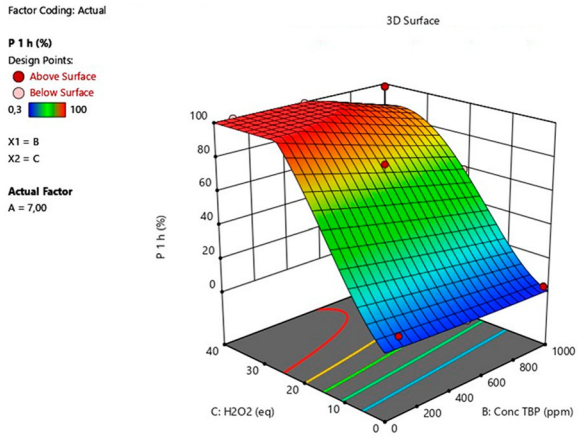

1. Introduction

Tributyl phosphate is an organophosphorus compound mainly used as flame retardant in the aircraft and automobile industry, and as an extraction agent for lanthanides in the nuclear industry in PUREX Process (Plutonium Uranium Refining by EXtraction). This process involves liquid–liquid extraction between TBP/dodecane (30/70) mixture and nitric acid solution. During the phases contacting, a hundred mg.L^{-1} of TBP can be solubilized into the aqueous phase [1], which has to be subsequently treated before discharge.

TBP has recently been identified and classified as a hazardous substance with harmful effects on aquatic life and humans, in whom it acts as an endocrine disruptor [2]. The limit in France for TBP release into rivers is therefore 50 µg.L^{-1} with a long-term flow threshold of 5 g per day. As this threshold is set to be reduced, new solutions for TBP degradation are required to reduce the concentration of pollutant out from the industry. Activated sludge treatment is the classical approach used in industrial effluent processing plants to degrade organic pollutants dissolved in water. A recent study on its application to OrganoPhosphorus

CONTACT Carine Julcour carine.julcour@ensiacet.fr Laboratoire de Génie Chimique, Université de Toulouse, CNRS, INPT, UPS, Toulouse, France
Supplemental data for this article can be accessed at https://doi.org/10.1080/09593330.2020.1751731.

Flame Retardants (OPFRs) in industrial effluent [3] highlighted the fact that these molecules are particularly bio-recalcitrant. New bacteria such as *Serratia odorifera* [4] and *Pseudomas pseudalcaligenes* [5] have been screened for their ability to degrade TBP: in 1–3 days of treatment from starting concentrations of 75–500 mg.L^{-1}, these strains were able to remove 31% to 73% of the TBP, respectively. This long and incomplete degradation, along with uncertainties regarding future threshold concentrations for bio-remediation and the fate of this compound in the environment, emphasize the requirement for complementary or alternative approaches.

Advanced Oxidation Processes (AOPs) are attractive in this context as their efficiency for the removal of refractory organic compounds is proven. The highly reactive and non-selective oxygen species such as hydroxyl radicals ($^{\bullet}$OH) generated in AOPs decompose the target compounds into non-toxic intermediates, such as short carboxylic acids, yielding CO_2, H_2O and mineral acids as final compounds. This contrasts with other powerful treatments such as chlorination, which produce toxic halides. Applying AOPs to industrial effluent treatment seems therefore to be a promising solution [6]. For TBP and similar molecules in particular, Cristale et al. [3] have shown for instance that an initial ozone concentration of 25 mg.L^{-1} can reduce the total OPFR content of industrial effluent treatment plant effluents by 25% to 50%. Similarly, using ultraviolet (UV)-C photocatalyzed β-Ga_2O_3, Seshadri and Sinha [7] were able to degrade 95% of the TBP in a 400 mg.L^{-1} solution in 30 min. Effective but slower removal was also achieved with a classical catalyst (TiO_2), with an equivalent degradation yield reached in 70 min [7,8], while Drinks et al. [8] degraded 87.5% of the TBP in a 100 mg.L^{-1} solution in 80 min using 0.5 g.L^{-1} TiO_2 and UV-A irradiation. The combination of UV light and H_2O_2 is a particularly interesting method of generating radicals because of its low cost and the easy availability of hydrogen peroxide. According to the review of Miklos et al. [9] UV/H_2O_2 appears among the most energy-efficient AOPs with E_{EO} (electrical energy per order) values in the order of 1 kWh/m^3 (compared to 100 kWh/m^3 or more for UV-based photocatalysis or ultrasound). Their study also revealed that this figure was influenced to some extent by water quality (median E_{EO} values ranging from 0.63 kWh/m^3 for drinking water to 2.2 kWh/m^3 for wastewater and 2.7 kWh/m^3 for ground water) and was reduced with an increase in scale (from 2.2 kWh/m^3 at lab-scale to 0.68 kWh/m^3 for pilot-scale and 0.5 kWh/m^3 for full-scale applications) [9]. Furthermore, the process is simple to manage, adaptable to changes in the influent [6,9] and industrial scale systems are available (Calgon Carbon's Peroxpure™ and Rayox® systems for drinking water treatment for instance).

There have been a few studies on the performance of the UV/H_2O_2 process for TBP remediation [3,10–12], but focussing on the disappearance of the molecule rather on its ultimate fate and the degradation process. The aim of the work reported here was to determine the degradation mechanism in full, as well as to examine the influence of key process parameters, such as the initial concentration of TBP, initial H_2O_2 concentration and initial pH.

2. Materials and methods

2.1. Reagents

The aqueous effluents originating from the nuclear fuel treatment contain the classical ions found in every water (bicarbonates, nitrates, sulphates, etc.). That is why all the experiments were performed in Evian water (composition in Table 1) to approximate the mineral content typically found in such industrial effluents and to insure a constant composition of the matrix.

Tributyl phosphate was purchased from Fluka with a purity of 99.8%. Hydrogen peroxide (H_2O_2) was purchased as a 35% w/w solution from Alfa Aesar.

Dibutyl phosphate (DBP) (≥97.0% purity, Sigma-Aldrich), a 1:1 DBP:MBP (mono butylphosphate) mixture (Alfa Aesar, molar ratio), phosphate, formate and acetate standards (1000 mg.L^{-1} supplied by Sigma Aldrich) were used to calibrate the quantitative ^{31}P NMR and ion chromatography analyses. All chemicals were used as received.

2.2. Experimental set-up and procedure

The laboratory scale photo-reactor used in this study consisted of a 1 L annular reactor (length: 38.2 cm; diameter: 6.3 cm) equipped with an immersion lamp in a quartz sleeve, and a recirculation loop. The content of the reactor was stirred magnetically at 450 rpm and the recycle flow rate was set to 164 L.h^{-1}, to ensure adequate mixing. The temperature inside the reactor was

Table 1. Mineral content of the Evian water used in the study.

Mineral	Concentration (mg.L^{-1})
HCO_3^-	360
Ca^{2+}	80
Cl^-	10
Mg^{2+}	26
NO_3^-	3.8
K^+	1
SiO_2	15
Na^+	6.5
SO_4^{2-}	14

kept at 20°C using a water-cooled jacket. The light source for the UV/H_2O_2 treatment was a low pressure mercury UV-C lamp (wavelength: 254 nm; radiation length: 33.7 cm; diameter: 2.3 cm) supplied by Heraeus. The photonic power of the lamp was measured with a UV radiometer using the Keitz method [13], resulting in a value of about 13 W. In complement, the photon flux entering the reactor was measured with the same captor, but directly at the quartz lamp holder wall, giving a value of $1.63 \cdot 10^{-5}$ ein.s^{-1}.

For the parametric study, the initial pH of the TBP solution was varied by adding H_2SO_4 or NaOH (1 M solutions). During the tests, pH value was not controlled, but its evolution was followed.

Tributyl phosphate is known be stable under acidic conditions (as in the PUREX process) and has been shown to remain stable for more than 30 days in slightly alkaline solutions [14]. The hydrolytic degradation of TBP was therefore assumed to be negligible over the pH range considered here.

The lamp was turned on 5 min before the injection of H_2O_2 to ensure the irradiation remained constant during the oxidation process. Samples (10 mL) were taken every 5 min for the first 30 min of the reaction, then at $t = 45$, 60, 150 and 360 min, and analysed using the methods described below.

2.3. Analytical methods

2.3.1. ^{31}P NMR

The organophosphorus species in the samples (TBP, DBP and MBP) were identified and quantified by ^{31}P NMR. NMR spectra were recorded on a Bruker 400 UltraShield VS spectrometer (161.976 MHz for ^{31}P) using deuterated water as the solvent with a dilution factor of 5. A total of 5632 scans were co-added for each sample. Internal calibration was performed from 5 to 100 mg.L^{-1} for DBP and from 1 to 100 mg.L^{-1} for the other phosphorous species. The precision of the analyses for TBP, DBP and MBP was 2% of the respective ranges.

2.3.2. Ion chromatography

Concentrations of phosphate and short-chain organic acids were measured using a Metrohm 930 Compact IC Flex ion chromatograph. The aliquots from the reactor were diluted 10-fold and 100 µL samples were injected into the device. The compounds were separated on a Metrosep A Supp 5 column maintained at 30°C and with the conductimetry detector set to 40°C. The mobile phase was 1 mM $NaHCO_3$ and 3.2 mM Na_2CO_3 in isocratic mode with a flow rate of 0.7 mL.min^{-1}. Calibration was performed using standards from 0.5 to 10 mg.L^{-1}. The overall uncertainty of the technique was estimated to be 2% over this concentration range.

2.3.3. Total organic carbon analysis

The mineralization of TBP was determined by measuring the residual total organic carbon (TOC) content of the samples, using a Shimadzu TOC-V device. The TOC data were also used to evaluate the contributions of identified organic compounds. The non-purgeable organic carbon method was used given the high concentrations of inorganic carbon, but the results were similar to the default (total carbon – inorganic carbon) method, ruling out any significant loss of light organic compounds during the measurements. Prior to injection (81 µL) the samples were diluted 10-fold, and 2% of a 2 M HCl solution was added to remove the inorganic carbon. The coefficient of variation between successive TOC measurements (three repetitions) was 5%.

2.3.4. Mass spectrometry

Mass spectrometry was used to identify other potential oxidation by-products such as butanol. The samples (500 µL) were injected directly at 500 µL.min^{-1} into a TSQ Quantum Access Max quadrupole device. The capillary temperature was 380°C and the electrospray temperature, 350°C. The analyses to detect butanol were performed in positive mode at a voltage of 2500 V.

2.3.5. Titration of remaining H_2O_2

The evolution of hydrogen peroxide concentration during the oxidation was followed by Eisenberg's method [15], where H_2O_2 forms a pertitanic acid complex with titanium (IV) salt under acidic conditions. Pertitanic acid is stable for a few hours and exhibits a yellow colour. This feature enables its concentration to be measured with a UV-Vis spectrometer set at 410 nm. Under these conditions, the molar absorption coefficient of pertitanic acid is 742 L.mol^{-1}.cm^{-1}.

In the course of the reaction, samples were withdrawn and diluted with ultra-pure water when required. Then, 50 mg of TiO_2 were mixed with 5 mL of H_2SO_4 at 98% and heated at 150°C for 16 h in order to obtain Ti^{4+} at 6.6 mmol.L^{-1}. 1 mL of this solution was mixed with 2 mL from the sample and produced the yellow complex.

This method allows the measurement of hydrogen peroxide concentration between 0.5 and 4.5 mM, the detection limit being 0.1 mM.

3. Results and discussion

3.1. Synergistic effect

No phosphate release was observed after 2.5 h when UV or H_2O_2 were used alone. The synergistic effects of UV and H_2O_2 on the degradation of TBP were then evaluated in terms of TOC removal, using apparent first-order constants (k). These experiments were performed at neutral initial pH with 100 mg.L^{-1} TBP and a H_2O_2/TBP molar ratio of 10. The synergy factor S was defined as shown in Equation (1).

$$S = \frac{k_{UV/H_2O_2}}{k_{UV} + k_{H_2O_2}} \quad (1)$$

The values obtained for $k_{H_2O_2}$, k_{UV}, and k_{UV/H_2O_2} were respectively ~0, 0.017, and 0.069 min^{-1}, with $S \approx 4$, highlighting the strong beneficial effect of combining UV and oxidant treatment. The facts that there was no TOC removal using H_2O_2 alone and minimal TBP photolysis prove that TBP degradation is mainly mediated by the photo-decomposition of H_2O_2 into radicals [16]. The absorption spectrum of 100 mg.L^{-1} TBP in Evian water (Figure S1, Supplementary Material), shows a molar absorption coefficient of 0.13 L.mol^{-1}.cm^{-1} at 254 nm (compared with about 20 L.mol^{-1}.cm^{-1} for H_2O_2).

3.2. Evolution of hydrogen peroxide concentration

The consumption of H_2O_2 concentration during TBP oxidation was followed for different oxidant amounts (from 10 to 60 molar equivalents with respect to TBP) starting with a TBP concentration of 100 mg.L^{-1} and an initial pH of 7.5. Figure 1 shows a similar time-conversion profile of the oxidant regardless of its initial concentration. Indeed, there should be a marginal competition for the photons in between TBP (poorly absorbing at 254 nm) and H_2O_2. In addition, the consumption of H_2O_2 was found almost complete after 30 min of oxidation and its possible scavenging effect should thus mainly prevail at the very beginning of the oxidation.

3.3. Degradation mechanism of TBP during UV/H_2O_2 treatment

The evolution of a typical ^{31}P NMR spectrum during oxidation is shown in Figure 2a. The chemical shifts of TBP, DBP, MBP and phosphate relative to 85% H_3PO_4 are −0.17, 0.9, 2.2 ± 0.2 and 3.4 ± 0.4 ppm, respectively. The small variation in the position of the MBP and phosphate peaks is an effect of initial pH changes during the reaction. Figure 2b shows that the concentration of TBP drops down to ~0 ppm in about 5 min, which is also

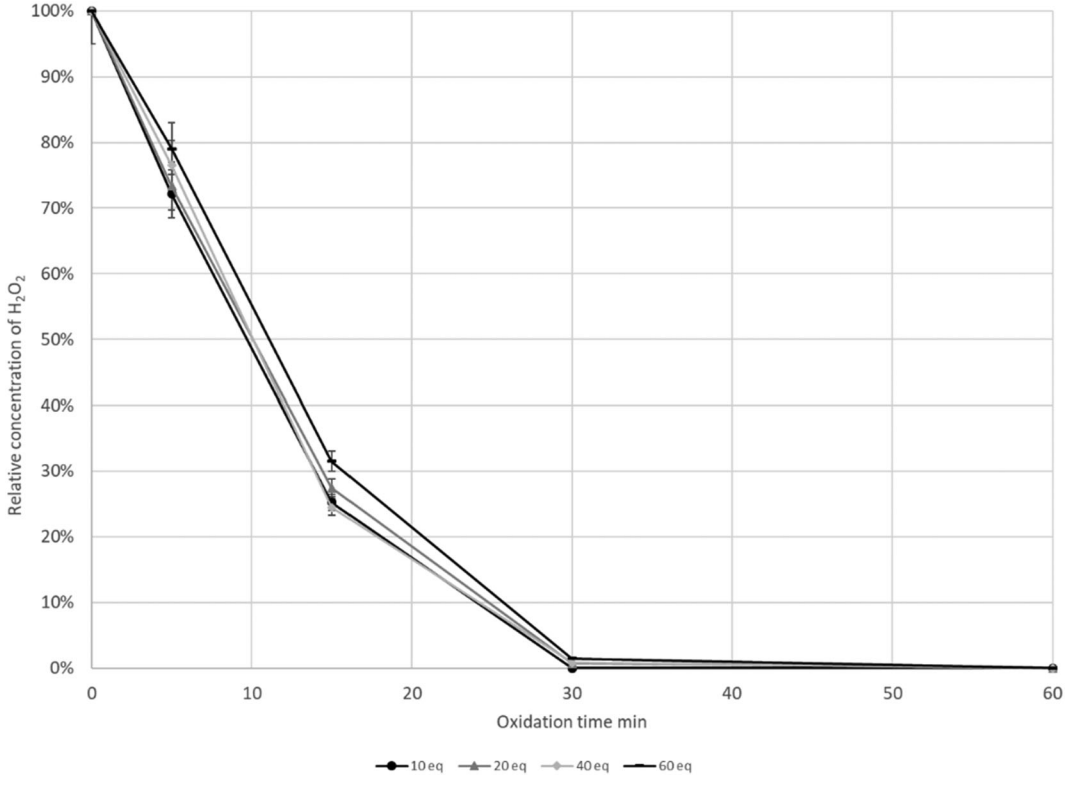

Figure 1. Consumption of H_2O_2 during the oxidation of 100 mg.L^{-1} TBP at $pH_0 = 7.5$ for different initial concentrations of H_2O_2 (expressed in molar equivalents with respect to TBP).

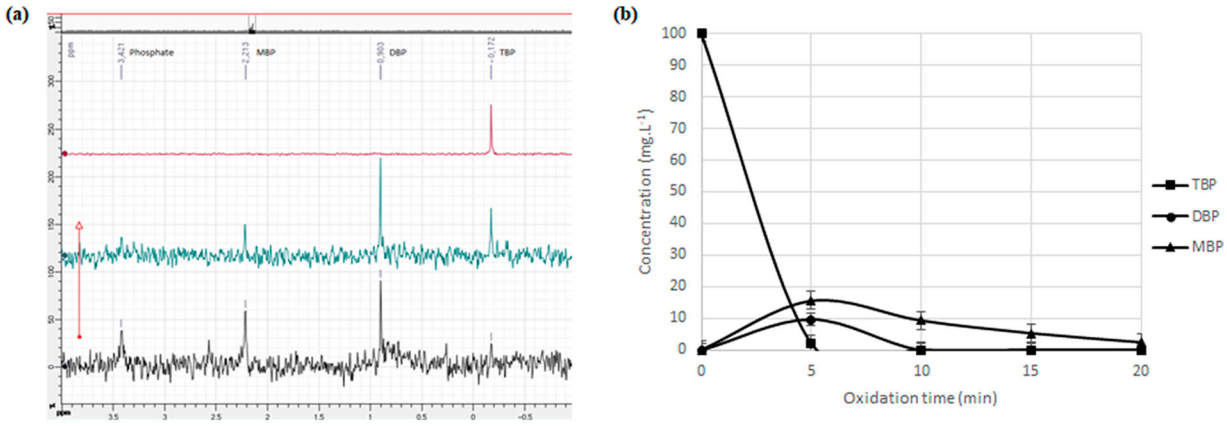

Figure 2. (a) ^{31}P NMR spectra of samples withdrawn at different times (red, 0 min; blue, 1 min; black, 2 min) during the oxidation of 100 mg.L^{-1} TBP at neutral initial pH and 20 molar equivalents of H_2O_2 ($[H_2O_2]_0$:$[TBP]_0 = 20$); (b) corresponding time-evolution of the concentration of the identified organophorphorus species (TBP, tributyl phosphate; DBP, dibutyl phosphate; MBP, monobutyl phosphate).

when the concentration of MBP and DBP are maximal (~16 and ~10 ppm, respectively).

Figure 3a shows the typical evolution of the chromatograms during UV/H_2O_2 treatment. At first, only the ions present in the Evian water are detected, namely chloride (rt = 8.5 min), nitrate (rt = 14.3 min) and sulphate (rt = 23 min), and their concentration remains stable throughout the reaction (Figure 3b). Under these operating conditions, acetate (rt = 6.5 min) and formate (rt = 7 min) ions appear within the first 15 min. Subsequently, oxalate ions (rt = 27 min) are formed and finally degraded, as the corresponding peak is no longer visible after 1 h. The molar absorption coefficients measured at 254 nm for the oxalate, acetate and formate reaction intermediates were 21.23, 0.02 and 0.12 L.mol^{-1}.cm^{-1}, respectively, while for TBP the value obtained was 0.13 L.mol^{-1}.cm^{-1}. Note that DBP, MBP and phosphate do not absorb at 254 nm. Oxalic acid has thus the same absorption coefficient as hydrogen peroxide, and might be readily photolyzed.

The pH showed a maximum variation by one pH unit from its initial value (cf. Figure 3b). This minimum corresponded to the highest concentration of formed carboxylic acids.

As mentioned in the introduction, the degradation/stability of TBP has already been studied under various treatments. The mechanism identified using alpha or gamma radiolysis by [17–19], with DBP and MBP as stable intermediates, has subsequently been observed under hydrolysis [20,21], thermal decomposition [22,23] and biodegradation [5,24]. Three butyl chains are detached one after the other, as shown in Figure 4 [8]. In aqueous solutions, the butyl phosphate species yield phosphate ions as the final phosphorus compound.

The fact that the corresponding species were all identified here (Figure 2a), confirms that the same mechanism applies under photo-oxidation. Regarding the fate of the carbon chains, butanol was only detected at trace levels by mass spectrometry (concentration < 0.1 mg.L^{-1}) in the early stages of process (at sampling times < 1 min). Among the six carboxylic acids targeted by ion chromatography, only acetic, oxalic and formic acid were identified (pyruvic, lactic and butyric acids were not found). The elemental balances of phosphorus and carbon were calculated (Equations (2) and (3), respectively) to confirm that the main oxidation intermediates had not gone undetected:

$$P_{\text{balance}} = \frac{[TBP]^t_{mol} + [DBP]^t_{mol} + [MBP]^t_{mol} + [PO_4^{3-}]^t_{mol}}{[TBP]^0_{mol}} \quad (2)$$

$$C_{\text{balance}} = \frac{TOC_{\text{identified species}}}{TOC_{\text{measured}}} \quad (3)$$

The values obtained at the different measurement times are listed in Table 2 at conditions yielding an intermediate oxidation rate. The phosphorus and carbon balances are both close to 100% at all the reaction times, confirming that that all major stable intermediates are identified. The small deviations from 100% are especially due to difficulties quantifying DBP below 5 mg.L^{-1}.

Figure 5 illustrates the mechanism proposed on the basis of these results for the oxidation of TBP during UV/H_2O_2 treatment. The alkyl chains detached from TBP are rapidly transformed into shorter C1–C2 carboxylic acids. As their concentration increases, the initial pH of the solution is slightly reduced, by about one unit at most. Oxalic acid appears last,

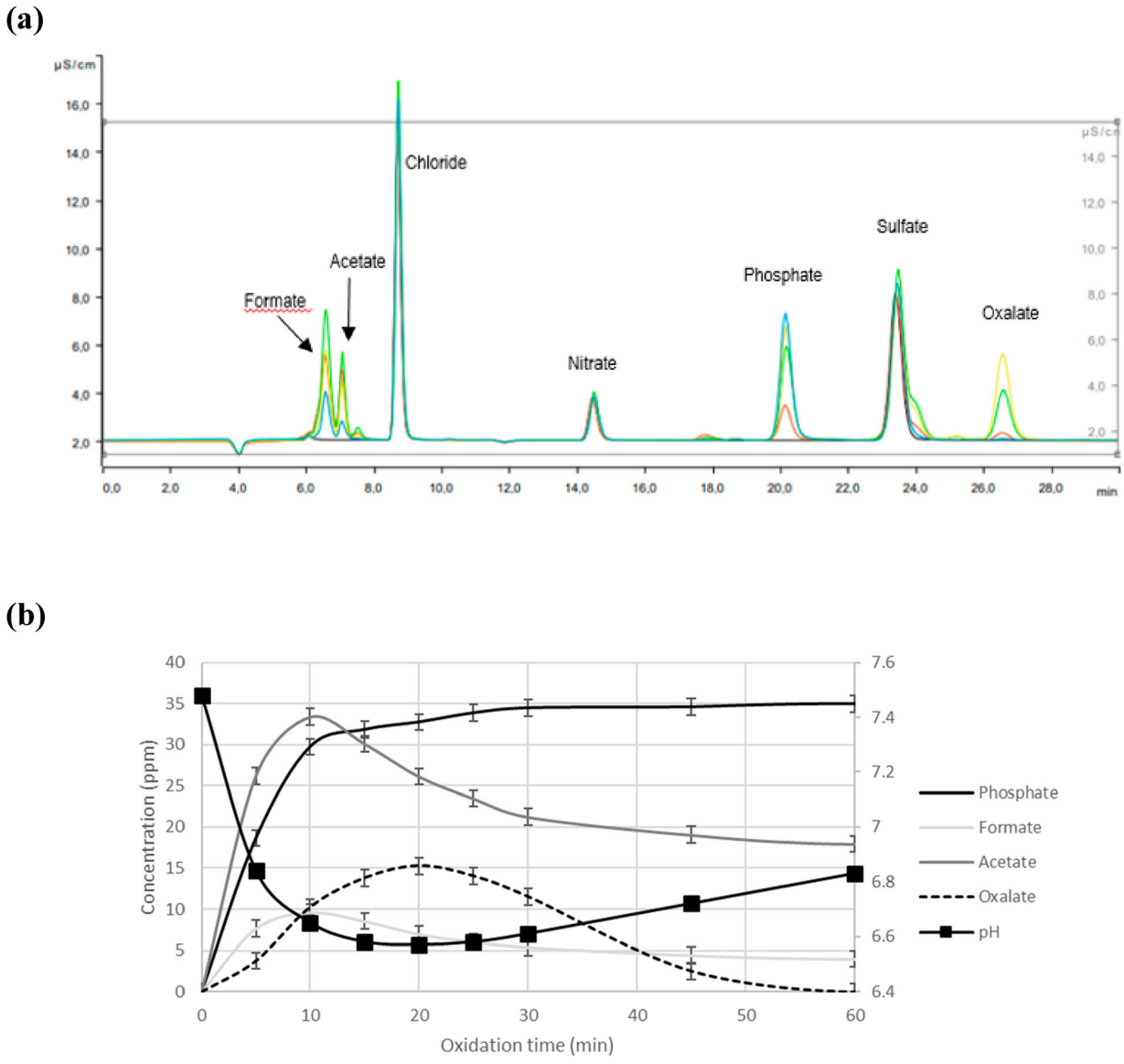

Figure 3. (a) Ion chromatograms of phosphate ions and light organic acids in samples withdrawn at different times (black, 0 min; red, 5 min; green, 10 min; yellow, 20 min; blue, 60 min) during the oxidation of 100 mg.L^{-1} TBP at a neutral initial pH and 20 molar equivalents of H_2O_2 ($[H_2O_2]_0$:$[TBP]_0 = 20$); (b) corresponding time-evolution of the concentration of carboxylic acids and phosphate.

probably from the oxidation of acetic acid. The concentration of acetic acid is the highest because of its low reactivity with hydroxyl radicals. Note that in their study of the UV-A photocatalysis of TBP, Drinks et al. [8] did not detect oxalic acid, but did identify C3–C4 acids (2-ketobutyric, propionic, lactic and pyruvic acid) not observed here. These differences can be ascribed to the stronger oxidizing conditions with UV/H_2O_2.

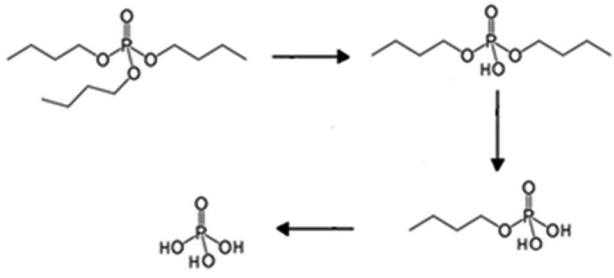

Figure 4. Structural formulas showing the sequence of four stages in the hydrolysis of tributyl phosphate.

3.4. Inhibition effect of hydrogen peroxide

Ultraviolet light activates the decomposition of H_2O_2 into $^{\bullet}OH$ radicals, which can subsequently oxidize organic compounds through different mechanisms. Several species, such as carbonate and phosphate ions [12,25,26], can compete with the pollutant for $^{\bullet}OH$ radicals, as can H_2O_2 itself when in large excess, according

to the following reactions:

$$^{\cdot}OH + H_2O_2 \rightarrow HO_2^{\cdot} + H_2O \quad (4)$$

$$HO_2^{\cdot} + {}^{\cdot}OH \rightarrow +H_2O + O_2 \quad (5)$$

The hydroperoxyl radicals ($HO_2^{\cdot}$) formed in the first reaction and consumed in the second one have a lower oxidation potential than $^{\cdot}OH$ (1.65 V *vs.* 2.8 V). There is therefore usually an optimal H_2O_2 concentration for peroxide-based AOPs and for UV/H_2O_2 process in particular [27].

To identify suitable boundaries for the experimental design optimization, a preliminary study was carried out to determine the maximum concentration of oxidant before inhibition occurs. The corresponding assays were performed at neutral initial pH (Evian water) with 100 mg.L^{-1} of TBP. Figure 6 shows the percentage of phosphate released as a function of the initial H_2O_2 concentration, expressed as H_2O_2/TBP molar ratio. Phosphate release levels off at 40 molar equivalents of H_2O_2, indicating that adding more hydrogen peroxide does not improve the degradation of TBP. At higher concentrations, the supplementary hydroxyl radicals are readily scavenged by the excess of peroxide and do not react with the pollutant [28–31]. The rate constant of the reaction between H_2O_2 and $^{\cdot}OH$ is 1.7–4.5 × 10^7 L.mol^{-1}.s^{-1}, which is about hundred times less than for the oxidation of TBP by $^{\cdot}OH$ (6.4 × 10^9 L.mol^{-1}.s^{-1} [11]), explaining the order of magnitude of excess concentration required for the competition effect to be observed.

3.5. Parametric study

The degradation process was optimized using a full factorial design with three factors (initial pH, initial TBP concentration and initial H_2O_2 concentration) and three levels for each [32]. Two assays were duplicated (5 and 9) and three additional intermediate conditions (I1-I3) were investigated. The parameter ranges covered were chosen based on preliminary observations or tests: the initial pH could not be increased above 8.5 because the magnesium ions in the Evian water precipitated as magnesium oxide, and the solubility limit of TBP was found to be above 1000 mg.L^{-1}. As discussed above, the reaction rate plateaued at H_2O_2 concentrations above 40 molar equivalents (Figure 6). Note that this concentration is only slightly more than the stoichiometric quantity required to mineralize the TBP according to:

$$PO(OC_4H_9)_3 + 36\ H_2O_2 = 3\ H^+ + PO_4^{3-} + 12\ CO_2 + 48\ H_2O \quad (6)$$

The selected limits of the parameters for the experimental design study are summarized in Table 3.

The degradation of TBP was assessed for each parameter combination by measuring the release of phosphate and the mineralization yield after 5, 15 and 60 min. These reaction times were selected based on the kinetics observed in preliminary experiments. The results obtained are shown in Table 4.

The fact that the absolute difference between replicates (5 vs 5R and 9 vs 9R) is less than 3% for the mineralization yields and less than 2.5% for phosphate release, shows that the results are reproducible.

The initial pH has a small to moderate effect on phosphate release and mineralization, with neutral or basic initial pH being preferable. Regardless of the initial pH or H_2O_2 concentration, the degradation process is usually less effective at higher pollutant concentrations, as is typically observed in AOPs [10,11,27]. This might be explained by some competition in between H_2O_2 and the formed by-products for the photons or by an increased amount of bicarbonate and phosphate ions formed during the mineralization.

The degradation efficiency is more strongly correlated with the H_2O_2 to TBP molar ratio. With an

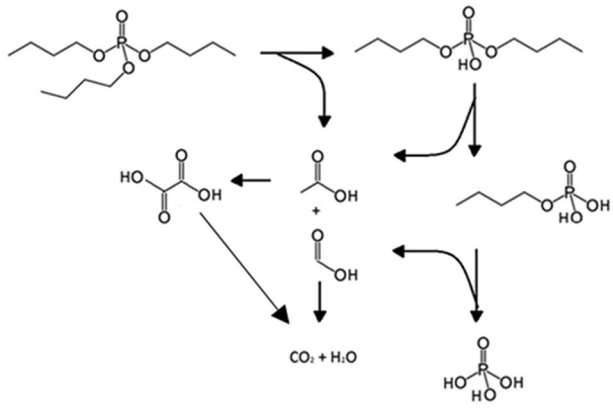

Figure 5. Structural formulas illustrating the proposed mechanism of tributyl phosphate degradation during UV/H_2O_2 treatment.

Table 2. Phosphorus and carbon balances during TBP oxidation by UV/H_2O_2 process (100 mg.L^{-1} TBP, neutral initial pH, 20 molar equivalents of H_2O_2).

t (min)	$P_{balance}$	$C_{balance}$ (TOC)
0	100%	100%
5	80%	85%
10	84%	91%
15	90%	95%
20	93%	99%
25	96%	94%
30	98%	100%
45	98%	100%
60	99%	100%
150	98%	100%
360	99%	100%

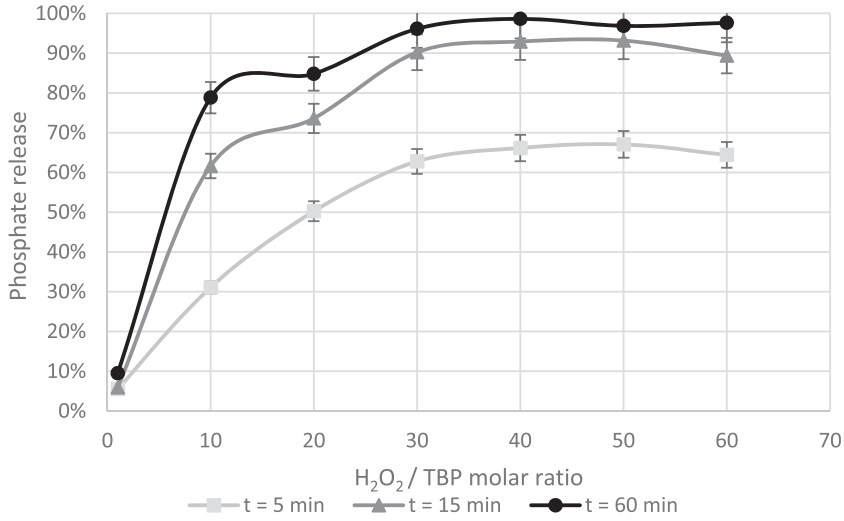

Figure 6. Percentage of phosphate released at different reaction times during the degradation of tributyl phosphate (TBP initial concentration: 100 mg.L^{-1}) by UV/H_2O_2 process at neutral initial pH: effect of the initial concentration of H_2O_2.

H_2O_2/TBP molar ratio of one, TBP is not significantly oxidized at any of the initial pH and initial concentrations investigated here. This may be because Evian water already contains a relatively high concentration of bicarbonate ions ($[HCO_3^-] = 360$ mg.L^{-1}), which can compete with TBP for $^{\bullet}OH$ groups at low radical concentrations. Note however that these ions should be removed at low initial pH, whereas as mentioned above, the process was actually more effective at neutral and basic initial pH.

To quantify the influence of the parameters more precisely and elucidate possible interaction effects, the responses were fitted with a quadratic model using the software Design Expert 11. The responses considered were phosphate release (Y_{PO_4}) and TOC removal (X) after 60 min, which vary substantially over the investigated range of operating conditions at this reaction time (Table 4).

The optimization led to the following equations for the percentages of phosphate release and TOC removal, respectively:

$$\sqrt{Y_{PO_4}\ (60\ \text{min})} = 2.133 + 0.022 \cdot \text{pH} - 0.0015 \cdot C_{TBP} + 0.479 \cdot D_{H_2O_2} - 0.0067 \cdot D_{H_2O_2}^2 \quad (7)$$

$$X\ (60\ \text{min}) = -\ 25.403 + 15.574 \cdot \text{pH} + 0.092 \cdot C_{TBP} + 0.244 \cdot D_{H_2O_2} - 0.0041\ \cdot \text{pH} \cdot C_{TBP} - 5.31 \cdot 10^{-4} \cdot C_{TBP} \cdot D_{H_2O_2} - 1.179 \cdot \text{pH}^2 - 6.90 \cdot 10^{-5} \cdot\ C_{TBP}^2\ + 0.033 \cdot D_{H_2O_2}^2 \quad (8)$$

Table 3. Parameters and selected levels for the experimental design study.

Initial TBP concentration (mg.L^{-1})	Initial pH	Initial H_2O_2 concentration (molar equivalent with respect to TBP)
100	2.15	1
500	7.5	20
1000	8.4	40

where $D_{H_2O_2}$ is the H_2O_2/TBP molar ratio and C_{TBP} is the pollutant concentration in mg.L^{-1}.

Accurate fits were obtained (see Figs S2 and S3, Supplementary Material) with adjusted coefficients of determination (which take into account the number of parameters in the equations) of 0.9772 and 0.9576 respectively, and predicted coefficients of determination of 0.9697 and 0.9358, respectively. The latter parameter is a cross-validation of the model, calculated by sequentially removing each of the data points and assessing how well the model fitted to the remaining data fits the missing point. The small differences (<0.03) between the adjusted and predicted coefficients show that the model is predictive and not overfit. Furthermore the high signal to noise ratio of the data ('Adeq Precision' > 20) and the low p-values of the models (<0.001) show that they are statistically significant and can be used over the design space.

The model for Y_{PO_4} confirms that increasing the TBP concentration has a negative effect on the degradation efficiency while higher initial pH and especially higher H_2O_2 concentrations are favourable. The model for X_{TOC} is more complex, with a greater number of interaction and quadratic terms.

The iso-response curves in Figure 7a reveal the influence of initial pH and TBP concentration on the

Table 4. Experimental results of the parametric study performed to optimize TBP degradation under UV/H_2O_2.

				Phosphate release (%)			Carbon mineralization yield (%)		
Test n°	Initial pH	$[TBP]_0$ (mg.L^{-1})	$[H_2O_2]_0$ / $[TBP]_0$ (molar ratio)	5 min	15 min	60 min	5 min	15 min	60 min
1	7	100	1	5.6	6.0	9.5	15.0	25.1	30.9
2	7	100	20	29.0	53.5	75.7	13.1	30.0	40.6
3	7	100	40	69.0	94.9	>99.9	28.3	70.5	95.2
4	7	500	1	1.1	1.2	1.9	15.7	26.3	43.9
5	7	500	20	9.6	36.0	76.2	25.3	36.7	57.2
5R	7	500	20	9.2	36.1	76.1	25.8	39.7	57.1
6	7	500	40	14.2	68.9	99.4	26.6	38.1	92.0
7	7	1000	1	1.0	1.4	2.2	2.1	13.8	19.9
8	7	1000	20	4.3	16.4	59.0	9.6	22.1	34.6
9	7	1000	40	11.0	42.2	98.3	3.9	34.0	55.8
9R	7	1000	40	13.2	40.1	99.4	5.4	36.5	58.2
10	2.15	100	1	2.5	4.8	10.8	2.2	9.8	13.9
11	2.15	100	20	13.1	58.1	81.3	20.1	25.5	33.3
12	2.15	100	40	41.6	87.7	>99.9	0.3	29.8	67.4
13	2.15	500	1	0.6	1.6	3.6	10.6	12.8	22.3
14	2.15	500	20	3.3	20.7	74.2	15.1	17.5	33.4
15	2.15	500	40	13.9	53.1	99.5	19.1	20.8	80.1
16	2.15	1000	1	0.0	0.2	0.3	2.0	7.4	20.1
17	2.15	1000	20	1.7	9.0	8.4	15.5	18.7	30.4
18	2.15	1000	40	12.5	37.6	97.6	9.5	34.4	55.2
19	8.4	100	1	3.6	5.4	8.1	16.9	29.0	32.1
20	8.4	100	20	21.8	70.2	98.8	15.1	31.7	40.0
21	8.4	100	40	58.3	88.6	99.5	24.7	64.0	86.5
22	8.4	500	1	0.6	1.2	2.2	26.5	30.7	31.4
23	8.4	500	20	6.7	36.5	76.4	29.4	38.7	45.0
24	8.4	500	40	14.6	67.0	99.2	14.2	26.0	94.4
25	8.4	1000	1	0.3	0.8	1.6	3.0	6.7	7.5
26	8.4	1000	20	3.3	15.2	50.4	13.1	13.7	18.7
27	8.4	1000	40	18.8	42.1	96.8	4.4	33.8	54.8
I1	7	300	40	39.8	74.6	93.6	15.4	45.8	93.6
I2	8.4	300	20	13.2	45.4	82.6	21.8	31.0	35.7
I3	2.15	100	10	0.85	4.6	5.4	8.8	13.1	25.3

degradation performance of the process at the maximum H_2O_2/TBP molar ratio. They confirm the positive effects of higher initial pH and lower TBP concentrations and show that complete phosphate removal can be achieved in 1 h for initial TBP concentrations up to 600 mg.L^{-1} (at neutral initial pH). Note that while much stronger scavenging effects are expected for carbonate than for bicarbonate ions, since the rate constant of their reaction with $^{\bullet}OH$ is almost two orders of magnitude higher: 3.9×10^8 *vs.* 8.5×10^6 L.mol^{-1}.s^{-1} [33] the maximum initial pH considered here is two units lower than the pKa of carbonate (10.3), which was therefore presumably not involved in these reactions. Likewise for the equilibrium between H_2O_2 and HO_2^- (whose molar absorptivity is much higher: 240 *vs.* 19.6 L.mol^{-1}.cm^{-1}), the former should predominate under the conditions investigated here because the pKa of HO_2^- is 11.6 [25,26].

Figure 7b shows the predictions of the model at neutral pH_0 (the most relevant in practice because modifying the pH of industrial effluent is costly and it promotes the conversion of TBP to DBP and MBP). Comparing the two parts of Figure 7 highlights the fact that the H_2O_2/TBP molar ratio has a much stronger effect on the TBP degradation efficiency than the pH_0 does. Increasing the H_2O_2 concentration always improves phosphate release regardless of the initial TBP concentration. The ideal parameter combinations to optimize phosphate release in 1 h are therefore a low TBP concentration (below 600 mg.L^{-1}) and a high H_2O_2/TBP molar ratio (35–40 eq).

The results for TOC removal (Figure 8) are similar. The effect of initial pH is stronger than it is for phosphate release (Figure 8a *vs.* Figure 7a), but as for the latter, the process is optimal (>90% TOC removal) for TBP concentrations below 600 mg.L^{-1}. The H_2O_2/TBP molar ratio has a stronger effect on carbon mineralization than the initial pH does (Figure 8a *vs.* Figure 8b). The optimal conditions at neutral initial pH are likewise a TBP concentration below 600 mg.L^{-1} and an H_2O_2/TBP molar ratio close to 40 eq.

The optimal ranges of the parameters are reported in Table 5 for all the investigated responses.

3.6. Degradation of TBP under optimal conditions

A 6 h validation test was performed with the optimal parameter combination (Figure 9). Under these conditions, the model predicted total phosphate release and a TOC removal of about 95% after 1 h. The experimental results are in accordance with these predictions (accounting for measurement uncertainties), with about 95% phosphate

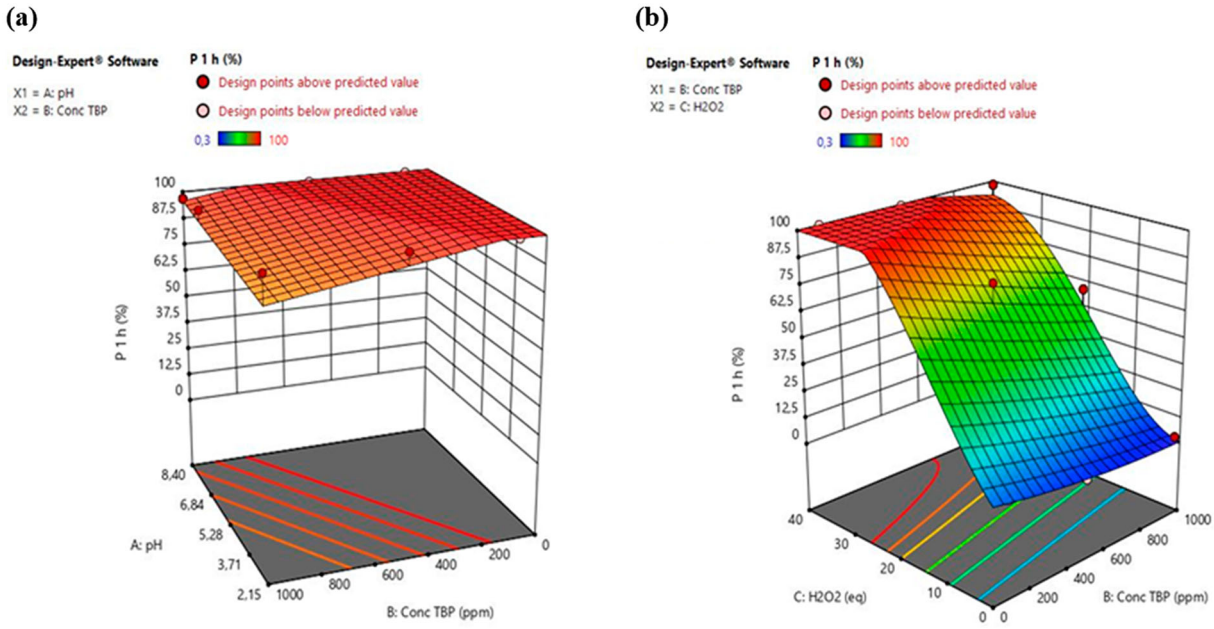

Figure 7. Influence of the design parameters on phosphate release after 1 h of TBP oxidation by UV/H_2O_2 process: (a) with the H_2O_2/TBP molar ratio set to 40 eq and (b) with $pH_0 = 7$.

release and 90% TOC removal at a reaction time of 1 h. From the above analysis (Figure 3b), the residual carbon after 1 h is probably in the form of acetic and formic acids.

Figure 9 shows that phosphate release is particularly rapid, reaching 75% in just 15 min. As the remaining carbon species are light carboxylic acids, which are easily digested by microorganisms, this process could be used as a short pretreatment before activated sludge processing. It may therefore be more relevant to focus only on the phosphate release.

High levels of phosphate release (>80%) could then be achieved in 1 h using a lower H_2O_2/TBP molar ratio (30 eq, Figure 10a). On the other hand, the fit of the phosphate response after 15 min (see also Figure S4, Supplementary Material) indicates that a yield of about 70% would be achieved for $[TBP]_0 < 400$ mg.L^{-1} and $[H_2O_2]_0/[TBP]_0 = 40$ (Figure 10b). This is an interesting perspective for future biodegradability analyses and ongoing initiatives to reduce oxidant usage, processing times, and thereby the cost of the treatment.

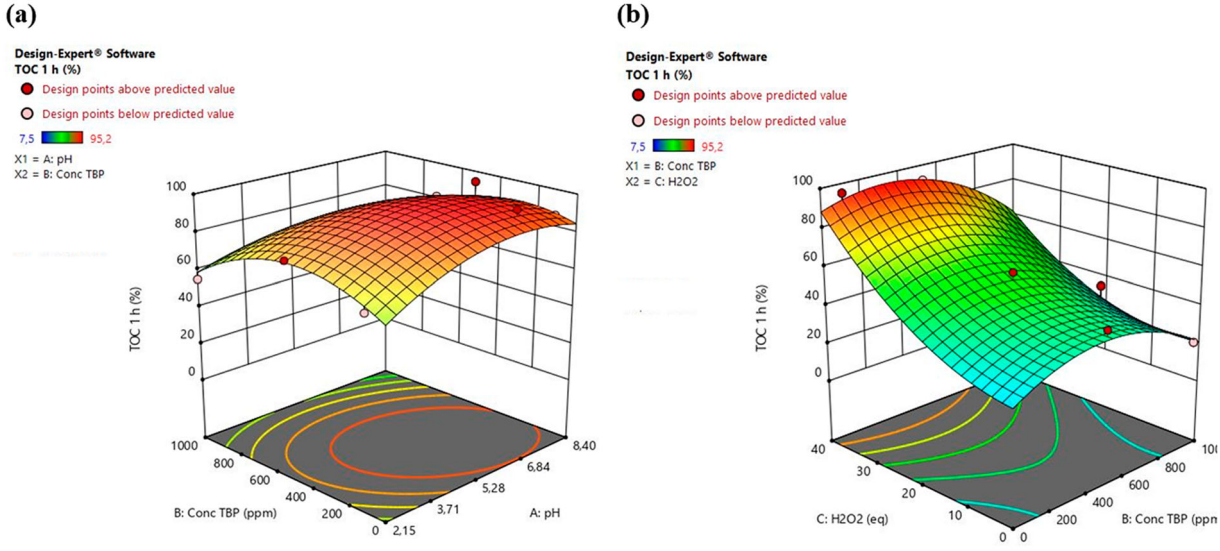

Figure 8. Influence of the design parameters on total organic carbon (TOC) removal after 1 h of TBP oxidation by UV/H_2O_2 process: (a) with the H_2O_2/TBP molar ratio set to 40 eq and (b) with $pH_0 = 7$.

Table 5. Optimal ranges of parameters from response surface methodology.

	Phosphate release			TOC removal		
Parameter	5 min	15 min	1 h	5 min	15 min	1 h
Initial pH	Weak impact	Weak impact	Weak impact	Basic	Basic	Neutral
Concentration of TBP	100 $mg.L^{-1}$	100-150 $mg.L^{-1}$	Up to 500 $mg.L^{-1}$	500 $mg.L^{-1}$	300 $mg.L^{-1}$	300 $mg.L^{-1}$
Initial H_2O_2 concentration (with respect to TBP)	40 eq	40 eq	40 eq	40 eq	40 eq	40 eq

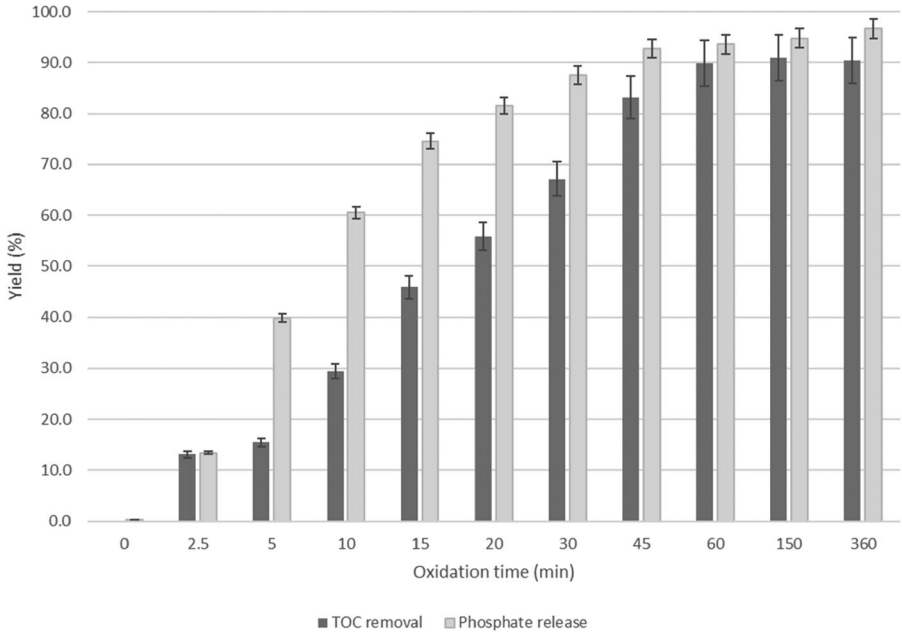

Figure 9. Evolution of phosphorus and carbon mineralization yields over 6 h during photo-oxidation of tributyl phosphate (TBP) starting with an initial concentration of 300 $mg.L^{-1}$, a neutral pH and H_2O_2/TBP molar ratio set at 40 eq.

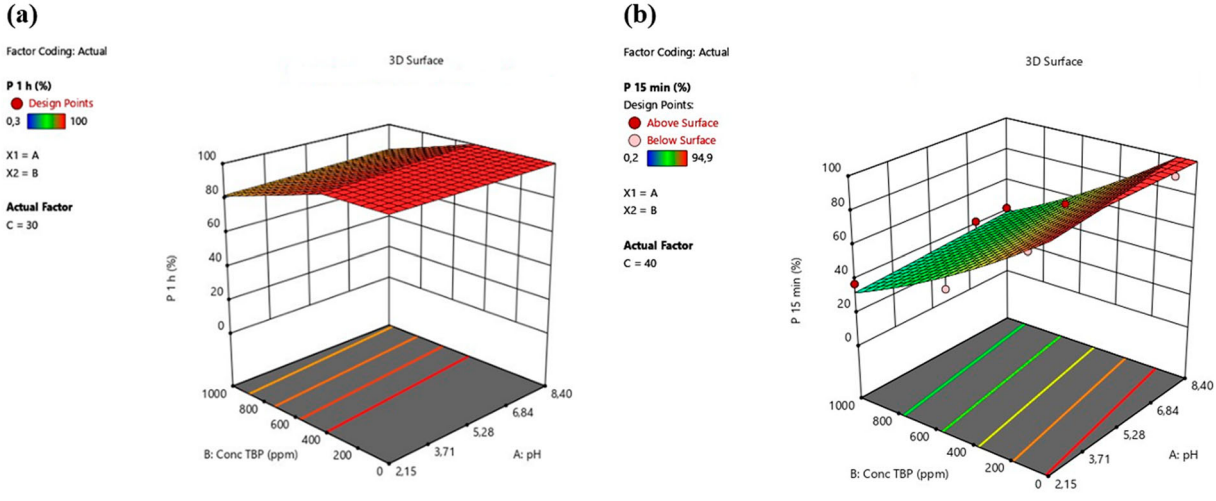

Figure 10. Phosphate release during TBP oxidation by UV/H_2O_2 process: (a) after 1 h with an H_2O_2/TBP molar ratio of 30; (b) after 15 min with an H_2O_2/TBP molar ratio of 40.

4. Conclusion

Ultraviolet/H_2O_2 treatment has been confirmed as a promising method for the removal of tributyl phosphate and is likely similarly effective for other organophosphorus compounds. Chromatography, NMR and TOC data show that after rapid phosphate release (~80% after 15 min under optimal conditions), the main organic intermediates are light carboxylic acids (acetic, formic and oxalic acid).

The concentration of H_2O_2 was the parameter that had the greatest effect on the efficiency of the process, with an H_2O_2/TBP molar ratio of 40 being optimal for both phosphate release and TOC removal, while avoiding wastage in competing reactions. Acidifying the reaction conditions did not prove beneficial and there was therefore little inhibition from bicarbonate ions. The process was shown to remain effective over a large range of TBP concentrations, up to 600 $mg.L^{-1}$, with more than two-thirds of the phosphate content released within 1 h. Phosphate release is achieved sooner than carbon mineralization for oxidant concentration near the stoichiometry, and lower H_2O_2 concentrations (e.g. a molar ratio of ~30) are required to achieve yields high enough to expedite subsequent sludge treatment, reducing operational costs. Having delineating the operating zone of interest in this study, biodegradability tests at different reaction times and operating conditions are in progress to help finalize the analysis.

Disclosure statement

No potential conflict of interest was reported by the author(s).

Funding

This work was supported by the French Alternative Energies and Atomic Energy Commission (CEA) [grant number 2017-THE-018-DE2D/SEAD/LPSD] and Occitania Region [grant number ALDOCT-000152].

References

[1] Velavendan P, Ganesh S, Pandey NK, et al. Studies on solubility of TBP in aqueous solutions of fuel reprocessing. J Radioanal Nucl Chem. 2013;295:1113–1117.
[2] ECHA. Tributyl phosphate – substance information – ECHA [Internet]. 2017 [cited 2019 Aug 18]. Available from: https://echa.europa.eu/fr/substance-information/-/substanceinfo/100.004.365
[3] Cristale J, Ramos DD, Dantas RF, et al. Can activated sludge treatments and advanced oxidation processes remove organophosphorus flame retardants? Environ Res. 2016;144:11–18.
[4] Berne C, Montjarret B, Guountti Y, et al. Tributyl phosphate degradation by Serratia odorifera. Biotechnol Lett. 2004;26:681–686.
[5] Chaudhari TD, Melo JS, Fulekar MH, et al. Tributyl phosphate degradation in batch and continuous processes using pseudomonas pseudoalcaligenes MHF ENV. Int Biodeterior Biodegrad. 2012;74:87–92.
[6] Parsons S, Byrne A. Advanced oxidation processes for water treatment: fundamentals and applications. London: IWA Publishing; 2004.
[7] Seshadri H, Sinha PK. Photocatalytic performance of combustion synthesized β-Ga_2O_3 for the degradation of tri-n-butyl phosphate in aqueous solution. J Radioanal Nucl Chem. 2012;292:649–652.
[8] Drinks E, Lepeytre C, Lorentz C, et al. UV-a photocatalytic degradation of the radionuclide complexants tributylphosphate and dibutylphosphate. Chem Eng J. 2018;352:143–150.
[9] Miklos DB, Remy C, Jekel M, et al. Evaluation of advanced oxidation processes for water and wastewater treatment – a critical review. Water Res. 2018;193:118–131.
[10] Watts MJ, Linden KG. Photooxidation and subsequent biodegradability of recalcitrant tri-alkyl phosphates TCEP and TBP in water. Water Res. 2008;42:4949–4954.
[11] Watts MJ, Linden KG. Advanced oxidation kinetics of aqueous trialkyl phosphate flame retardants and plasticizers. Environ Sci Technol. 2009;43:2937–2942.
[12] Santoro D, Raisee M, Moghaddami M, et al. Modeling hydroxyl radical distribution and trialkyl phosphates oxidation in UV–H_2O_2 photoreactors using computational fluid dynamics. Environ Sci Technol. 2010;44:6233–6241.
[13] Rekab K, Lepeytre C, Dunand M, et al. H_2O_2 and/or photocatalysis under UV-C irradiation for the removal of EDTA, a chelating agent present in nuclear waste waters. Appl Catal Gen. 2014;488:103–110.
[14] Wright A, Paviet-Hartmann P. Review of physical and chemical properties of tributyl phosphate/diluent/nitric acid systems. Sep Sci Technol. 2010;45:1753–1762.
[15] Eisenberg G. Colorimetric determination of hydrogen peroxide. Ind Eng Chem Anal Ed. 1943;15:327–328.
[16] da Silva SW, Heberle ANA, Santos AP, et al. Antibiotics mineralization by electrochemical and UV-based hybrid processes: evaluation of the synergistic effect. Environ Technol. 2019;40:3456–3466.
[17] Williams TF, Wilkinson RW. Radiolysis of tri-n-butyl phosphate. Nature. 1957;179:540.
[18] Burger LL, McClanahan ED. Abstract of the American Chemical Society Meeting. Miami, Fla; 1957.
[19] Burr JG. The radiolysis of tributyl phosphate. Radiat Res. 1958;8:214–221.
[20] Davids W, Kibbey A. Aqueous-phase decomposition of TBP at 35–75°C in nitric acid solutions. ORNL Rep. 1970; ORNL-TM3062:1–20.
[21] David MD, Seiber JN. Accelerated hydrolysis of industrial organophosphates in water and soil using sodium perborate. Environ Pollut. 1999;105:121–128.
[22] Powell BA, Navratil JD, Thompson MC. Compounds of hexavalent uranium and dibutylphosphate in nitric acid systems. Solvent Extr Ion Exch. 2003;21:347–368.
[23] Patil LK, Gaikar VG, Kumar S, et al. Thermal decomposition of nitrated Tri-n-butyl phosphate in a flow reactor [Internet]. Int Sch Res Not. 2012. [cited 2018 Mar 20]. Available from: https://www.hindawi.com/journals/isrn/2012/193862/
[24] Nancharaiah YV, Kiran Kumar Reddy G, Krishna Mohan TV, et al. Biodegradation of tributyl phosphate, an organosphate triester, by aerobic granular biofilms. J Hazard Mater. 2015;283:705–711.
[25] Sillanpää MET, Agustiono Kurniawan T, Lo W. Degradation of chelating agents in aqueous solution using advanced oxidation process (AOP). Chemosphere. 2011;83:1443–1460.
[26] Muruganandham M, Suri RPS, Jafari S, et al. Recent developments in homogeneous advanced oxidation

processes for water and wastewater treatment [Internet]. Int J Photoenergy. 2014. [cited 2018 Jan 10]. Available from: https://www.hindawi.com/journals/ijp/2014/821674/

[27] Li M, Li W, Bolton JR, et al. Organic pollutant degradation in water by the vacuum-ultraviolet/ultraviolet/H_2O_2 process: inhibition and enhancement roles of H_2O_2. Environ Sci Technol. 2019;53:912–918.

[28] Cater SR, Stefan MI, Bolton JR, et al. UV/H_2O_2 treatment of methyl tert-butyl ether in contaminated waters. Environ Sci Technol. 2000;34:659–662.

[29] Lopez-Alvarez B, Villegas-Guzman P, Peñuela GA, et al. Degradation of a toxic mixture of the pesticides carbofuran and iprodione by UV/H_2O_2: evaluation of parameters and implications of the degradation pathways on the synergistic effects. Water Air Soil Pollut. 2016;227:215.

[30] Liu Z, Hosseinzadeh S, Wardenier N, et al. Combining ozone with UV and H_2O_2 for the degradation of micropollutants from different origins: lab-scale analysis and optimization. Environ Technol. 2019;40:3773–3782.

[31] Somathilake P, Dominic JA, Achari G, et al. Influence of UV dose on the UV/H_2O_2 process for the degradation of carbamazepine in wastewater. Environ Technol. 2019;40:3031–3039.

[32] Córdova RN, Nagel-Hassemer ME, Matias WG, et al. Removal of organic matter and ammoniacal nitrogen from landfill leachate using the UV/H_2O_2 photochemical process. Environ Technol. 2019;40:793–806.

[33] Buxton GV, Greenstock CL, Helman WP, et al. Critical review of rate constants for reactions of hydrated electrons, hydrogen atoms and hydroxyl radicals ($^{\bullet}OH/^{\bullet}O^{-}$) in aqueous solution. J Phys Chem Ref Data. 1988;17:513–886.

Supplementary Material

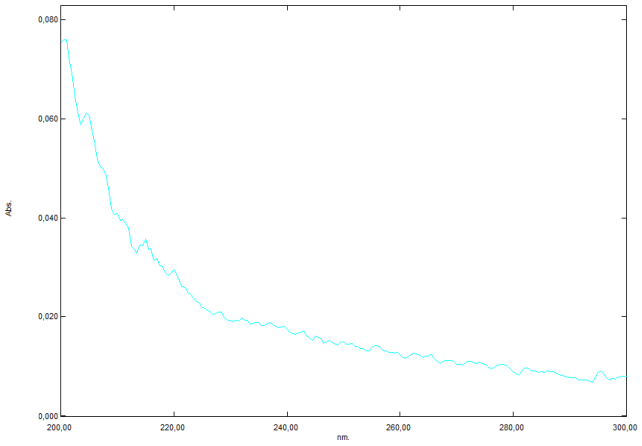

Fig. S1. Absorption spectrum of 100 ppm TBP in Evian water (cuvette width, 10 mm).

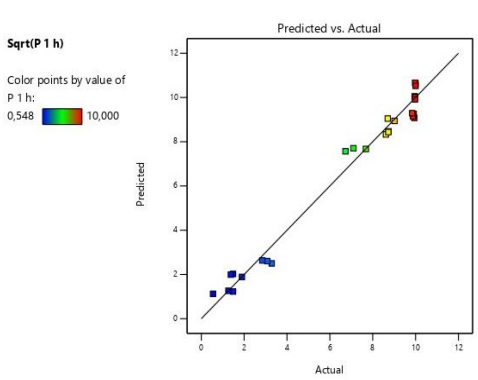

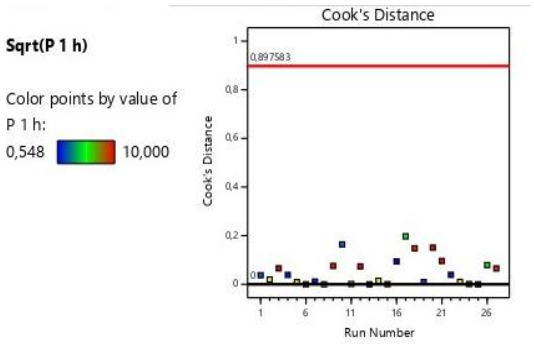

Source	Sum of Squares	df	Mean Square	F Value	p-value Prob > F
Model	333.9700	4	83.4900	279.8600	0.0001
A-pH	0.0913	1	0.0913	0.3059	0.5858
B-Conc TBP	8.5300	1	8.5300	28.5800	0.0001
C-Eq H2O2	305.8000	1	305.8000	1025.0500	0.0001
C^2	38.4500	1	38.4500	128.9000	0.0001
Residual	6.5600	22	0.2983		
Cor Total	340.5300	26			

Std. Dev.	0.5462
Mean	6.7400
C.V. %	8.1000

R-Squared	0.9807
Adj R-Squared	0.9772
Pred R-Squared	0.9697
Adeq Precision	40.5729

(P release 60min)^{0,5}	=
2.133590	
0.021709	* pH
-0.001526	* Conc TBP
0.479000	* Eq H2O2
-0.006663	* Eq H2O2 ^{2}

Model	Significant
A-pH	Non Significant
B-Conc TBP	Significant
C-Eq H2O2	Significant
C^2	Significant
Std. deviation	Significant
Adequation	Significant
Precision	Significant

$$\sqrt{Y_{PO4}\ (60\ \text{min})} = 2.13 + 0.022 \cdot pH - 0.0015 \cdot C_{TBP} + 0.479 \cdot D_{H_2O_2} - 0.0067 \cdot D_{H_2O_2}^2$$

Fig. S2. Output of the fitting software Design Expert 11 for the reduced quadratic model of phosphate release after 1h.

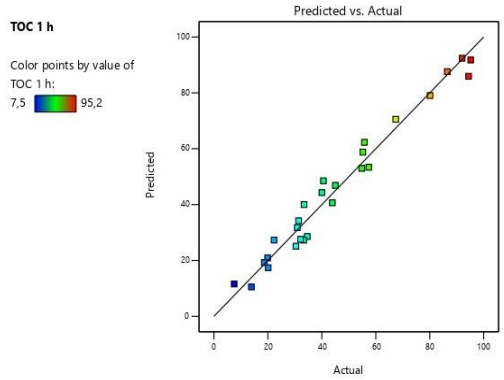

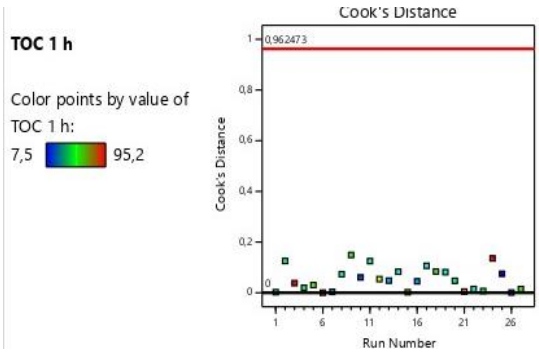

Source	Sum of Squares	df	Mean Square	F Value	p-value Prob > F
Model	16595.9600	8	2074.4950	74.4900	0.0001
A-pH	211.4400	1	211.4400	7.5900	0.0130
B-Conc TBP	199.4400	1	199.4400	7.1600	0.0154
C-Eq H2O2	11243.8900	1	11243.8900	403.7200	0.0001
AB	433.6300	1	433.6300	15.5700	0.0009
BC	261.2500	1	261.2500	9.3800	0.0067
A^2	349.2100	1	349.2100	12.5400	0.0023
B^2	1125.3700	1	1125.3700	40.4100	0.0001
C^2	935.8000	1	935.8000	33.6000	0.0001
Residual	501.3200	18	27.8511		
Cor Total	17097.2800	26			

Std. Dev.	5.2800
Mean	45.8100
C.V. %	11.5200

R-Squared	0.9707
Adj R-Squared	0.9576
Pred R-Squared	0.9358
Adeq Precision	26.8683

TOC removal 60min	=
-25.402910	
15.574030	* pH
0.092403	* Conc TBP
0.244197	* Eq H2O2
-0.004065	* pH * Conc TBP
-0.000531	* Conc TBP * Eq H2O2
-1.179240	* pH ²
-6.90E-05	* Conc TBP ²
0.032868	* Eq H2O2 ²

Model	Significant
A-pH	Significant
B-Conc TBP	Significant
C-Eq H2O2	Significant
AB	Significant
BC	Significant
A^2	Significant
B^2	Significant
C^2	Significant
Std. deviation	Non Significant
Adequation	Significant
Precision	Significant

$$X\ (60\ \text{min}) = -25.403 + 15.574 \cdot pH + 0.092 \cdot C_{TBP} + 0.244 \cdot D_{H_2O_2} - 0.0041 \cdot pH \cdot C_{TBP} - 5.31 \cdot 10^{-4} \cdot C_{TBP} \cdot D_{H_2O_2} - 1.179 \cdot pH^2 - 6.90 \cdot 10^{-5} \cdot C_{TBP}^2 + 0.033 \cdot D_{H_2O_2}^2$$

Fig. S3. Output of the fitting software Design Expert 11 for the reduced quadratic model of TOC removal after 1h.

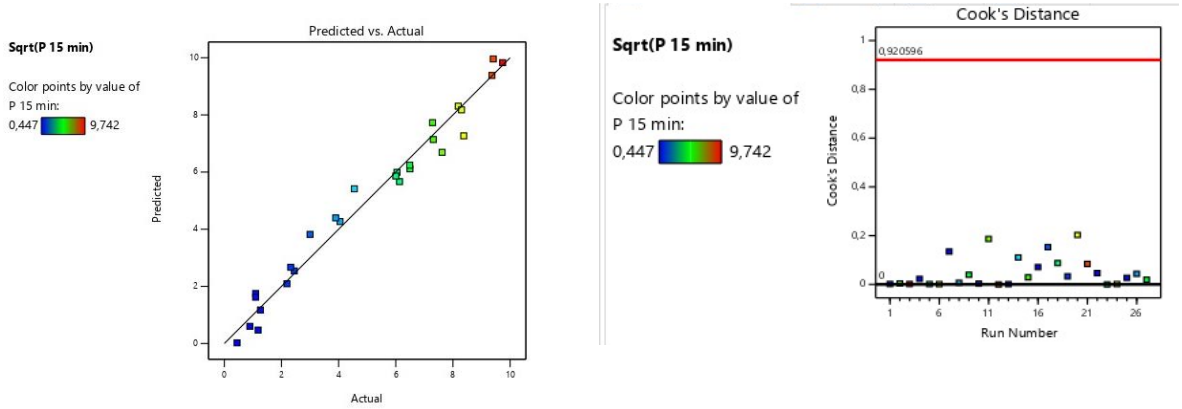

Source	Sum of Squares	df	Mean Square	F Value	p-value Prob > F
Model	236.7700	5	47.3500	154.2300	0.0001
A-pH	1.6500	1	1.6500	5.3800	0.0306
B-Conc TBP	37.2200	1	37.2200	121.2300	0.0001
C-Eq H2O2	196.2000	1	196.2000	638.9900	0.0001
BC	2.0400	1	2.0400	6.6500	0.0175
C^2	6.5800	1	6.5800	21.4400	0.0001
Residual	6.4500	21	0.3070		
Cor Total	243.2100	26			

Std. Dev.	0.5541
Mean	5.0100
C.V. %	11.0700

R-Squared	0.9735
Adj R-Squared	0.9672
Pred R-Squared	0.9559
Adeq Precision	38.0325

(P release 15min)^0.5	=
1.821930	
0.092345	* pH
-0.002251	* Conc TBP
0.304611	* Eq H2O2
-4.70E-05	* Conc TBP * Eq H2O2
-0.002757	* Eq $H2O2^2$

Model	Significant
A-pH	Significant
B-Conc TBP	Significant
C-Eq H2O2	Significant
BC	Significant
B^2	Significant
Std. deviation	Significant
Adequation	Significant
Précision	Significant

$$\sqrt{Y_{PO4}\,(15\ min)} = 1.822 + 0.092 \cdot pH - 0.0023 \cdot C_{TBP} + 0.305 \cdot D_{H_2O_2} - 4.70 \cdot 10^{-5} \cdot C_{TBP} \cdot D_{H_2O_2} - 0.0028 \cdot D_{H_2O_2}^2$$

Fig. S4. Output of the fitting software Design Expert 11 for the reduced quadratic model of phosphate release after 15 min.